The game of 15 sticks in *E. coli*

R. Andreev & H. Hu

2021-02-01

1 Introduction

1.1 The game of 15 sticks[1]

We design genetic circuits in *E. coli* that play the following game:

> Two players start with 15 sticks and alternatingly take 1, 2 or 3 sticks.
> The last player to take a stick loses.

1.2 General design

We encode in binary the number of sticks left as

$$\text{number of sticks left} = 8\,\mathsf{s}_3 + 4\,\mathsf{s}_2 + 2\,\mathsf{s}_1 + \mathsf{s}_0. \tag{1}$$

By the 4-periodicity of the winning strategy (see §1.4), only the two lowest bits $\mathsf{s}_1/\mathsf{s}_0$ matter to the player. The response of a player is a number 1, 2, or 3, which we encode in binary as

$$\text{number of sticks taken by a player} = 2\,\mathsf{r}_1 + \mathsf{r}_0. \tag{2}$$

The bits in (1)–(2) are transmitted between compute units by intercellular signaling molecules, cf. §1.5. Although our players are essentially identical, we model them separately with one difference: Player A (B) becomes active when the extracellular signal w_A (w_B) is supplied.

The *Subtractor* module keeps track of the number of sticks left (1). To appreciate the key design issue, suppose we manually transmit the response $\mathsf{r}_1\,\mathsf{r}_0 = \mathsf{01}$ of a player into the medium of the subtractor. It should compute the new number of the sticks, yet, it has to do so once and not keep subtracting the value $\mathsf{r}_1\,\mathsf{r}_0$ that is still present. One solution is single-use subtractors but then the result of each computation has to be imparted to an unused one. A feasible design seems to require some separation of reading/storing the current state, computing the new state and communicating it – temporally or spatially. We propose a

[1] Cite as: The game of 15 sticks in *E. coli*, R. Andreev & H. Hu, 2021-02-01, http://bit.ly/15sticks. See the link for the codes and the PDF file with sharp figures. Thanks to: Y. Benenson and M. Chen.

subtractor composed of two parts A and B, and a workflow as shown in Table 1. Thus, in Phase A characterized by the supply of the master signal $\mathsf{w_A}$, Subtractor A emits the current state s, Player A responds with r, while Subtractor B reads s/r and computes the new state silently and remembers the result in order to emit it in the subsequent Phase B. We use the variables $\mathsf{d_3}/\mathsf{d_2}/\mathsf{d_1}/\mathsf{d_0}$ for this internal state. The medium is cleared, before Phase B is initiated by supplying the master signal $\mathsf{w_B}$. Briefly, we require a gated memory module and a delayed response, cf. §1.4.

	Phase A	Interphase I	Phase B
Experimenter	supply $\mathsf{w_A}$	clear medium	supply $\mathsf{w_B}$
Player A	in: s, out: r	–	–
Subtractor A	out: new s	–	in: s/r; compute
Subtractor B	in: s/r; compute	–	out: new s
Player B	–	–	in: s, out: r

Table 1: Workflow: Phases I/A/I/B alternate until the game is over.

1.3 Conventions

As shown in Table 4, we encode $\mathsf{w_A}$ by L-arabinose, $\mathsf{w_B}$ by IPTG, etc. Our convention is $\mathsf{w_A} = 1$ if the corresponding messenger molecule L-arabinose is present in the medium/cell in sufficiently high quantity, and $\mathsf{w_A} = 0$ otherwise. We write $\#\mathsf{w_A}$ for the *number* of L-arabinose molecules in the numerical simulations. Where suitable, we indicate the semantics of an element thus: $\langle\mathsf{signal}\rangle$, $(\mathsf{protein})$ – often a transcription factor, and $[\mathsf{promoter}]$; this is consistent with the symbols that we employ in the SimBiology schemes. By $\langle\mathsf{w_A}\rangle$ we mean "the signal molecule that encodes $\mathsf{w_A}$", i.e. L-arabinose. Ditto for the other signals.

Abbreviations: RBS = ribosome binding site, QS = quorum sensing, AHL = acyl homoserine lactone, 3OC6 = 3OC6-HSL (etc.), SM = supplementary material, DNF = disjunctive normal form, txn = transcription, TF = transcription factor.

1.4 Logic circuits

Player. Both players follow the same deterministic strategy, which is a winning strategy for the first-mover. They are identical except that player A responds when $\mathsf{w_A}$ is present and player B responds upon $\mathsf{w_B}$. The logic is shown in Table 2.

Subtractor. In Phase A, Subtractor B senses the current number of sticks (1), emitted by Subtractor A, and the response (2) from Player A, and computes the difference d. It has four compute units Bit 0 to Bit 3 that are also spatially separated (cf. §1.5). The subtraction proceeds from Bit 0 to Bit 3. Bit 0 senses the current $\mathsf{s_0}/\mathsf{r_0}$ and computes $\mathsf{d_0}$ (silently) and the carry flag $\mathsf{c_1}$ (emitted immediately). The carry flag is passed on to Bit 1. Bit 1 subtracts

r_1 and c_1 from s_1. The resulting carry flag c_2 is passed on to Bit 2, which subtracts c_2 from s_2. Then Bit 3 subtracts the resulting carry flag c_3 from s_3. Each Bit 0/2/3 is in fact a "half-subtractor" with 2 inputs, whilst Bit 1 is a "full subtractor" with 3 inputs. See Table 3 for their truth table. Fig. 7 shows a reference logic circuit for Bit 0 and Bit 1 that illustrates the principle of delayed response.

Since Bits 0/2/3 are a subfunctionality of Bit 1, we will not discuss them in detail.

Winning strategy marked with a star:

Sticks left				Take
15	11	7	3	$2^\star$
14	10	6	2	$1^\star$
13	9	5	1	1
12	8	4		$3^\star$

w_A	s_1	s_0	r_1	r_0
0	0	0	0	0
0	0	1	0	0
0	1	0	0	0
0	1	1	0	0
1	0	0	1	1
1	0	1	0	1
1	1	0	0	1
1	1	1	1	0

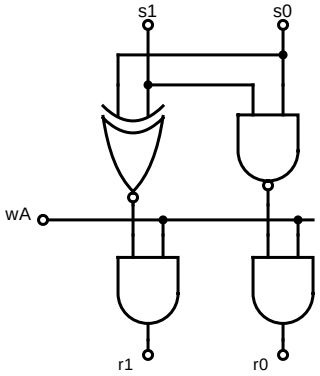

Table 2: Both players follow the same strategy. Truth table and logic circuit for Player A. The input is a wake-up signal w_A and the bits s_1/s_0 of the current number of sticks (1). The output is the number of sticks taken (2). The output is cut off unless w_A is present. The circuit for Player B is identical except that the output is controlled by w_B.

Half-subtractor:

s_3	c_3	d_3	–
s_2	c_2	d_2	c_3
s_0	r_0	d_0	c_1
0	0	0	0
0	1	1	1
1	0	1	0
1	1	0	0

s_1	r_1	c_1	d_1	c_2
0	0	0	0	0
0	0	1	1	1
0	1	0	1	1
0	1	1	0	1
1	0	0	1	0
1	0	1	0	0
1	1	0	0	0
1	1	1	1	1

$$\begin{aligned} & 8\,s_3 + 4\,s_2 + 2\,s_1 + s_0 \\ - \quad & 2\,r_1 + r_0 \\ = \quad & 8\,d_3 + 4\,d_2 + 2\,d_1 + d_0 \end{aligned}$$

Table 3: The subtractor computes $d = s - r \pmod{16}$. As r only has these two bits, a half-subtractor is sufficient for the bits $d_0/d_2/d_3$ and the carry flags c_1/c_3, and only d_1/c_2 require the full subtractor. We have $d_0 = (s_0 \,\mathsf{XOR}\, r_0)$; $c_1 = \mathsf{not}(s_0 \geq r_0)$; $d_1 = ((s_1 + r_1 + c_1) \bmod 2)$; $c_2 = \mathsf{not}(s_1 \geq r_1 \geq c_1)$. See Fig. 7 for a logic circuit.

1.5 Experimental design

We distinguish *extracellular* chemical signals that are supplied by the experimenter (the master signals w_A/w_B) and *intercellular* signals that are produced and sensed by cells. For an experiment in a single test tube we need orthogonal intercellular channels: *three* for (1)

(s_3 has no downstream), *two* for (2), and *three* for the carry flags (see §1.4). Thus we need *eight* orthogonal intercellular channels. One channel could be spared at the expense of a more involved computation of the last useful carry flag c_3. Du et al. (2020) designed ten de novo intercellular signaling pathways and optimized four known QS pathways. However, only *eight* worked well orthogonally on the sensor level and *seven* on the promoter level (Du et al., 2020, Fig. 3c/g). We have assigned in Table 4 the signals to minimize crosstalk, in particular avoiding LuxR and RpaR in one cell, heeding the advice of Du et al. (2020, p.6).

	⟨signal⟩, (txn factor), [promoter]	Primary reference	Details
w_A	⟨Ara⟩ → (AraC*) → [BAD]	Nielsen et al. 2016, SM:VII.M	§2.5/p.6
w_B	⟨IPTG⟩ ⊣ (LacI) ⊣ [Tac]	Nielsen et al. 2016, SM:VII.M	§2.5/p.6
r_0	⟨3OC6-HSL⟩ → (LuxR) → [Lux*]	Du et al. 2020, SM:p.3	§2.6/p.7
r_1	⟨IV-HSL⟩ → (BjaR) → [Bja*]	Du et al. 2020, SM:p.2	§2.6/p.7
s_0	⟨DAPG⟩ ⊣ (PhlF) ⊣ [PhlF]	Du et al. 2020, SM:p.3	§2.6/p.7
c_1	⟨Sal⟩ → (NahR) → [Sal]	Du et al. 2020, SM:p.3	§2.6/p.7
s_1	⟨pC-HSL⟩ → (RpaR) → [Rpa*]	Du et al. 2020, SM:p.2	§2.6/p.7
c_2	⟨MMF⟩ ⊣ (MmfR) ⊣ [Mmf*]	Du et al. 2020, SM:p.2	§2.6/p.7
s_2	⟨3OC12-HSL⟩ → (LasR) → [Las*]	Du et al. 2020, SM:p.3	§2.6/p.8
c_3	⟨NG⟩ → (FdeR) → [FdeA]	Du et al. 2020, SM:p.3	§2.6/p.8

Table 4: Extra-/intercellular ⟨signals⟩ with downstream (factors) and [promoters].

To facilitate debugging we partition the workflow into six spatial compartments (for example, 10 mL centrifuge tubes) that require manual transmission of the medium: two for the players (A and B) and four for the subtractor (Bits 0–3). Unfortunately, this does not automatically reduce the number of intercellular channels needed. Each Bit compartment contains two subpopulations of cells as part of Subtractor A or B, referred to as Bit 0A, Bit 0B, etc.

To initialize the experiment, add ⟨w_B⟩ with ⟨s_i⟩ to each Bit i, causing Subtractor A to compute and remember $d_i = 1$. Then wash and replace the medium. In Phase A, do the following steps, adding ⟨w_A⟩ before each step.

1. Having added ⟨w_A⟩ to Bit 0 and Bit 1, wait for emission of s_1 and s_0.
2. Admix the media from Bits 0/1 containing s_0/s_1 to Player A, wait for response. Note, the medium may or may not contain the actual signal molecules ⟨s_0⟩/⟨s_1⟩.
3. Admix the medium from Player A containing r_0/r_1/s_0/s_1 to Bit 0. Wash Player A, replenish with fresh medium. Wait for: Bit 0B to compute the difference d_0 (silent); Bit 0A to compute the carry flag c_1.
4. Admix the medium from Bit 0 containing c_1 to Bit 1. Wash and replenish Bit 0. Wait for: Bit 1B to compute the difference d_1 (silent); Bit 1A to compute the carry flag c_2.
5. Admix the medium from Bit 1 containing c_2 to Bit 2.x Wash and replenish Bit 1. Wait for: Bit 2B to compute the difference d_2 (silent); Bit 2A to compute the carry flag c_3.

6. Admix the medium from Bit 2 containing c_3 to Bit 3. Wash and replenish Bit 2. Wait for Bit 3B to compute the difference d_3 (silent). Wash and replenish Bit 3.

This concludes Phase A. In the interphase it may be necessary to clear the media again and generally wait for the steady state. Phase B proceeds similarly. The game finishes when the internal states d are zero. We can detect this, for example, by coupling expression of reporter proteins to the memory units (details omitted).

Refinements could include a) dealing with a player who attempts to take more sticks than (1); b) dedicated sensor cells that report on signaling molecules in order to monitor the communication channels; c) cells that emit $\langle \mathsf{s}_3 \rangle / \langle \mathsf{s}_2 \rangle / \langle \mathsf{s}_1 \rangle / \langle \mathsf{s}_0 \rangle$ upon one signal, e.g. tetracycline, in order to reboot the game.

2 Genetic toolbox

2.1 Constitutive parts

Constitutive promoter. The iGEM part BBa_J23100 is a strong constitutive *E. coli* σ^{70} promoter. We refer to it as P_c (or a close variant thereof).

cI. The optimized and orthogonal variants $\mathsf{cI}^a := \mathsf{cI}_{\mathsf{opt}}$ and $\mathsf{cI}^b := \mathsf{cI}_{\mathsf{5G6G,P}}$ of the transcription factor λ cI from (Brödel et al., 2016, Fig. 4c/d) require no cofactors and show about 10-fold activation of their "forward" promoter ($[\mathsf{cI}^a_+]$ and $[\mathsf{cI}^b_+]$) and a similar-fold repression of their "backward" promoter ($[\mathsf{cI}^a_-]$ and $[\mathsf{cI}^b_-]$). Arkin et al. (1998) performed a detailed stochastic computational analysis of the phage λ lysis-lysogeny decision circuit.

2.2 3-input gates by Cello

Nielsen et al. (2016) reported among the good performers: $\mathsf{r}_0 = \mathsf{0x0E}(\mathsf{s}_0, \mathsf{s}_1, \mathsf{w}_\mathsf{A})$; $\mathsf{r}_1 = \mathsf{not}\,\mathsf{0xF6}(\mathsf{s}_0, \mathsf{s}_1, \mathsf{w}_\mathsf{A})$; $\mathsf{c}_2 = \mathsf{not}\,\mathsf{0x8E}(\mathsf{c}_1, \mathsf{r}_1, \mathsf{s}_1) = \mathsf{0x4D}(\mathsf{c}_1, \mathsf{s}_1, \mathsf{r}_1)$, which is symmetric in $\mathsf{r}_1/\mathsf{c}_1$; but we couldn't find the 3-XOR, see §2.9.

We used their 0x0E for r_0, replacing the sensors and replacing the repressor PhlF (which clashes with the s_0 sensor) by HlyIIR (also from (Nielsen et al., 2016)). The last operation is a "poor man's OR gate"; we let it control (cI^a) (§2.1) that triggers the synthesis of $\langle \mathsf{r}_0 \rangle$. We observed that r_1 can reuse most of this circuitry and implemented the remainder using ribocomputing (details omitted). For c_2, we took not 0x8E, replacing the sensors and replacing the final "not(not(·) OR not(·))" by a ribo-AND gate with cross-inhibition (see §2.8/p.9).

2.3 Intracellular pathways (transducers)

AmtR. The TetR-like AmtR regulates the nitrogen starvation response in the Gram-positive *C. glutamicum* (Jakoby et al., 2000). This repressor is released by the trimeric

adenylylated signaling protein GlnK (Beckers et al., 2005; Sevvana et al., 2017), which is present upon nitrogen starvation. The AmtR box and the regulon is characterized in (Beckers et al., 2005) and several variants are compared in (Muhl et al., 2009). It seems clear that AmtR sits on the DNA as a dimer (Sevvana et al., 2017), (Schwab, 2019, §3.4.2).

Further, we use the transcription repressors BetI and HlyIIR, see (Nielsen et al., 2016).

2.4 Insulation of genetic context and RBS

To reduce "part-junction interference" and maintain relative promoter strengths, Lou et al. (2012) (and Nielsen et al. (2016)) inserted a ribozyme just upstream of the RBS, which cuts off the 5'-UTR leader sequence and the scar, if present. This remedies early saturation of transcription (Lou et al., 2012, SM:Fig. 5) and thus increases the choice of RBS for regulating expression on the translation level (Lou et al., 2012, SM:Fig. 4), (Salis, 2011). An additional hairpin helps expose the RBS (Lou et al., 2012; Carrier and Keasling, 1997). Insulating sequences can also be placed upstream of promoters (including [BAD]) to reduce order dependence (Carr et al., 2017).

For our purposes, standard RBS sequences such as BBa_J61100 can be used.

2.5 Extracellular signaling

Recall that the two master signals w_A/w_B are encoded by L-arabinose/IPTG. Following Nielsen et al. (2016, SM, VII.M) we posit a truncated (AraC*) that has reduced crosstalk with IPTG. The sequences can be found in (Nielsen et al., 2016, SM, Table S8) for (Ara*) and (LacI), and in (Nielsen et al., 2016, SM, Table S9) for [BAD] and [Tac].

2.6 Intercellular pathways

Here we collect key aspects of the intercellular receivers. 3OC6, IV and 3OC12 belong to the AHL QS family, whereas pC has a p-coumaric acid group rather than a fatty acyl group. According to Hirakawa et al. (2011, p.2598), LuxR homologs (which function as homoserine lactones receivers) are homodimeric. Du et al. (2020) used the LuxR and LuxR homologs LasR (Fuqua et al., 1996, Table 1), RpaR (Hirakawa et al., 2011, p.2598), BjaR (Lindemann et al., 2011). The TetR family are transcriptional repressors that sit on the operons and block the corresponding promoters (Ramos et al., 2005). The repression are released by specific inducers (often antibiotics) via a conformational change. It is suggested (Ramos et al., 2005; Cuthbertson and Nodwell, 2013) that the TetR-type proteins are usually homodimers with two slots for the inducer. PhlF and MmfR are TetR homologs. Of note, Du et al. (2020, SM:p.8) reported that sender cells enter the log-phase with delay compared to control samples (Sal, DAPG: ≈12h; 3OC6, 3OC12, pC, MMF: ≈3h; IV, NG: no delay). See (Du et al., 2020, SM) for sequences, biosynthesis and induction curves.

3OC6. The transcription activator LuxR occurs in Gram-negatives such as *V. fischeri*, that is permeable to the (auto)inducer 3-oxo-C6-homoserine lactone ⟨3OC6-HSL⟩. It binds to the N-terminal of (LuxR), which otherwise inhibits its functional C-terminal (Stevens et al., 1994). The purified C-terminal binds upstream of the *lux* box (which is centered at −42.5bp (Egland and Greenberg, 1999)); however, together with the RNA Pol, it protects the *lux* box and the *lux* operon promoter (Stevens et al., 1994).

IV. Isovaleryl-HSL (IV) is a branched-chain fatty acyl-HSL from soybean symbiont *B. japonicum* that regulates (BjaR). In the presence of IV, dimerized BjaR activates [Bja] (Lindemann et al., 2011).

DAPG. 2,4-diacetylphloroglucinol (DAPG) is a broad-spectrum antibiotic phenol produced by some Gram-negative *P. fluorescens*. Bangera and Thomashow (1999) identified the phlABCD operon (in strain Q2-87) required for the synthesis of 2,4-DAPG and its precursor MAPG. This operon is flanked by genes phlE (efflux protein) and phlF (repressor protein, (Bangera and Thomashow, 1999, p.3162)), which are separately transcribed. The helix-turn-helix motif of phlF resembles that of the TetR-family (Bangera and Thomashow, 1999, p.3161). Schnider-Keel et al. (2000) investigated auto-induction of DAPG synthesis (in strain CHA0), and reported, in particular, strong repression by extracellular ⟨Sal⟩ (indeed, *P. fluorescens* has a NahR-homolog HQ912_21075); but the phlF mutant was unaffected by it. CHA0 also contains the gene phlG to specifically degrade DAPG to MAPG (Bottiglieri and Keel, 2006).

We use PhlF as the transcription factor repressed by DAPG. Du et al. (2020, Fig. 2a) use the gene cluster PhlABCD for the synthesis of DAPG.

Sal. The transcription activator (NahR) binds to the recognition site of [Sal] at −83 to −45 without the inducer (Huang and Schell, 1991, p.10837), (Schell and Wender, 1986). Schell et al. (1990) suggested that the active configuration of (NahR) is a tetramer, while Park et al. (2005) reported that there could be three different complexes (NahR) : [Sal]. Possibly (Peking iGEM 2013 team, 2013), 4×(NahR) bind to the DNA, and transcription starts once a ⟨Sal⟩ binds to each (NahR).

pC. The transcription factor RpaR protein senses P-coumaroyl-HSL with p-coumaric acid rather than fatty acids. Hence, it shows good orthogonality to many AHL-HSL receiver proteins (Schaefer et al., 2008). The *R. palustris* transcriptional regulator RpaR, when purified, binds an inverted repeat element centered at −48.5bp of its promoter (Hirakawa et al., 2011). The complex ⟨pC⟩ : (RpaR) bound to the promoter activates transcription (Hirakawa et al., 2011, Discussion).

MMF. Methylenomycin furans (Mmf) are precursors of methylenomycin, an antibiotic produced by *S. coelicolor* (Zhou et al., 2020). As a TetR-family transcriptional regulator,

MmfR represses [Mmf], but accumulation of ⟨Mmf⟩ releases it (O'Rourke et al., 2009). The TetR homolog MmfR forms a homodimer (Zhou et al., 2020), which contains two Mmf recognition sites. Different R-groups of Mmfs may alter the binding affinity (Zhou et al., 2020, p.2-3). Du et al. (2020, p.2) use an MMF with a branched side chain.

3OC12. Two 3-oxo-dodecanoyl-homoserine lactone (3OC12-HSL) molecules bind irreversibly to the dimerized (LasR) from *P. aeruginosa*. The activated LasR activates several promoters with high affinity with no or positive cooperativity (Schuster et al., 2004; Grant et al., 2016). Du et al. (2020, p.2) use a custom promoter [Las*].

NG. Naringenin (NG) is the main flavone from grapefruits (Siedler et al., 2014; Hein et al., 2014). It binds the homodimeric protein FdeR from *H. seropedicae*. There are two slots for NG, whose binding induces a conformational change of the dimer. The activated FdeR promotes the "Flavanone degradation" operon [FdeA].

2.7 Memory module

As explained in §1.2 (cf. Table 1/3 and Fig. 7), we need a memory module to record and recall the result of the subtraction. To that end we use a "reversible" recombinase. Specifically, the Bxb1 gp35/gp47 serine-integrase/excisionase (Int/Xis) direct the infection cycle of Bxb1 in *M. smegmatis*. Stoichiometry, start codons, degradation rates (proteolysis tags) and DNA substrate copy number were optimized in *E. coli* in (Bonnet et al., 2012) to assemble a memory bit that is stable and responsive over several generations. A promoter of choice is flanked by Int recognition sites and its direction is *set* by Int and *reset* by Int+Xis. Switching times of ∼4h were demonstrated but the authors expected 30min to be realistic. Their final construct (Bonnet et al., 2012, Fig. 4A) consists of an Int gene and a Xis+Int operon induced by two separate signals, which facilitates stoichiometry optimization. However, in our design, an external pulse (say, $\langle w_B \rangle$) controls Int, and an internal compute unit (say, s_0 XOR r_0) controls Xis. The *reset* state corresponds to positive output, i.e. the memory bit is *on*. The flanked promoter is activated by another external signal (say, $\langle w_A \rangle$).

2.8 Enhanced AND gate

HrpR/HrpS. Wang et al. (2011, Fig. 1) proposed an AND gate in *E. coli* using the heterodimeric transcription factor HrpR : HrpS from *P. syringae*. The dimer binds upstream of the promoter hrpL and opens the σ^{54}-RNAP-hrpL transcription complex. Increasing the copy number of this weak promoter improves the dynamic range (Wong et al., 2015, p.4).

Ribocomputing. Green et al. (2017, Fig. 2e) combined short RNAs A and B into a "trigger" RNA which opens an RBS-occluding stemloop on the output mRNA (cf. Fig. 1c).

Cross-inhibition. Even in our idealized simulations such AND gates produce undesirable leakage within larger circuits. We propose that *low* input a inhibit the downstream of b, and vice versa: we let $\mathsf{a} \to \mathsf{cI}^a$ and $\mathsf{b} \to \mathsf{cI}^b$ produce two orthogonal bidirectional transcription factors as in §2.1. They, in turn, activate $[\mathsf{cI}^a_+]/[\mathsf{cI}^b_+]$ and repress $[\mathsf{cI}^a_-]/[\mathsf{cI}^b_-]$:

$$\left.\begin{array}{l} \mathsf{B}^* \overset{\text{txn}}{\leftarrow} [\mathsf{cI}^a_-] \vdash (\mathsf{cI}^a) \to [\mathsf{cI}^a_+] \overset{\text{txn}}{\to} \mathsf{A} \\ \mathsf{A}^* \overset{\text{txn}}{\leftarrow} [\mathsf{cI}^b_-] \vdash (\mathsf{cI}^b) \to [\mathsf{cI}^b_+] \overset{\text{txn}}{\to} \mathsf{B} \end{array}\right\} \to \overset{\text{trigger RNA}}{\mathsf{AB}} \to \begin{array}{c}\text{opens RBS on} \\ \text{the output mRNA.}\end{array} \tag{3}$$

Herein, A and B form a trigger RNA AB as in (Green et al., 2017, Fig. 2e), including toeholds for preferential binding of the complementary RNAs A^* and B^*. The cross-inhibition is more effective if $[\mathsf{cI}^a_-] > [\mathsf{cI}^b_+]$ and $[\mathsf{cI}^b_-] > [\mathsf{cI}^a_+]$ in terms of the output of the promoters.

2.9 3-input XOR

The subtractor result bit (cf. Table 3 and §2.2)

$$\mathsf{d}_1 = \mathsf{0x69}(\mathsf{s}_1, \mathsf{r}_1, \mathsf{c}_1) = \mathsf{not}\,\mathsf{0x96}(\mathsf{s}_1, \mathsf{r}_1, \mathsf{c}_1) = \mathsf{3\text{-}XOR}(\mathsf{s}_1, \mathsf{r}_1, \mathsf{c}_1) = ((\mathsf{s}_1 + \mathsf{r}_1 + \mathsf{c}_1) \bmod 2) \tag{4a}$$

$$= (s_1 \wedge \overline{\mathsf{r}_1} \wedge \overline{\mathsf{c}_1}) \vee (\overline{\mathsf{s}_1} \wedge \mathsf{r}_1 \wedge \overline{\mathsf{c}_1}) \vee (\overline{\mathsf{s}_1} \wedge \overline{\mathsf{r}_1} \wedge \mathsf{c}_1) \vee (\mathsf{s}_1 \wedge \mathsf{r}_1 \wedge \mathsf{c}_1) \tag{4b}$$

is particularly difficult because the result flips whenever any input is flipped. It is a concatenation of two XOR gates (cf. Fig. 7). We considered:

- Cascading two XOR gates built on tandem promoters as in (Nielsen et al., 2016, Fig. 3).
- Cascading two XOR gates, each as in (Wong et al., 2015, Fig. 5) but with two orthogonal heterodimeric transcription activators (cf. §2.8).
- RNA AND-gates as in Fig. 1b instead of the protein heterodimer.
- RNA-only gate inspired by (Green et al., 2017, Fig. 2e). Each input expresses its own mRNA, whose 5' tail opens its RBS stemloop. Each input also expresses complementary RNAs that sequester other tails thus closing up other RBS. Upon all three inputs, all complementary RNAs form a ring, so that the 5' tails reopen their RBS.
- Three orthogonal resettable recombinases as in (Chiu and Jiang, 2017, Fig. 2g).
- Cas13/ribozymes to cut mRNA instead of zipping up the RBS as in the final design.
- The recombinase-based (Weinberg et al., 2017) and the multi-cell (Ausländer et al., 2017) one-bit adders, mentioned here for completeness.

Eventually, we implemented the DNF (4b) using RBS switches. Each input signal produces 1) an output mRNA; 2) two short RNAs that inhibit the output mRNA of the other two inputs using the "three-way junction" mechanism of (Kim et al., 2019, Fig. 1c); 3) a co-trigger RNA: upon all 3 signals, the co-trigger RNAs form a trimer that opens the RBS of a fourth (constitutively transcribed) output mRNA as in (Green et al., 2017, Fig. 2e).

Fig. 2 shows the corresponding genetic circuits:

- The first circuit constitutively provides the transcription factors to sense the signals s_1 (pC-HSL), r_1 (IV-HSL) and c_1 (Sal).
- The second circuit is activated by pC-HSL through four independent promoters [Rpa*] (the copy number and strength of each may have to be tuned): two kinds of inhibitory trigger RNAs (bd and cd), one "co-trigger" RNA mk and an output mRNA. The trigger RNA bd / cd inhibits the output from the IV-HSL / Sal responsive circuit as in Fig. 1a.
- IV-HSL and Sal responsive circuits work analogously. Thus, the output from the responsive circuits is translated if exactly one of the inducers is present.
- Another copy of output mRNA is constitutively transcribed but is silenced by its RBS stemloop by default. Only when the 3 co-trigger RNAs form a trimer, the exposed sequence mn pries open the RBS, see Fig. 1c. Therefore, the output is expressed when all 3 signals are present.

2.10 Shelving

The 3-XOR gate from §2.9 activates or represses translation of an output mRNA. We take this output to be the transcription factor cI^a that activates the expression of a trigger RNA Y with toehold, which in turn triggers the translation of Xis. Thus, the presence of Y stands for $d_1 = 1$. Now, suppose $\mathsf{w_B} = 1$ and $\mathsf{s_1\, r_1\, c_1} = 101$, in which case $\mathsf{d_1} = 0$. Then Y is low, but around the timepoint when $\mathsf{w_B}$ is turned off and the inputs begin to change, Y can exhibit a transient bump (which we observed in some simulations). This can cause production of Xis and an unintended *reset*. One way to mitigate this is to condition the expression of Xis on $\mathsf{w_B}$ as well, which requires $\mathsf{w_B}$ to go down early and also tuning of degradation rates. We implemented another, complementary way, which is a "shelf" (a buffer) for Y that i) has high affinity for Y; ii) sequesters about $30\times\mathrm{EC50}_{\mathsf{Y}\,\to\,\mathsf{Xis}}$ copies of Y; iii) is degraded when $\mathsf{w_A}$ is on. In this way, a transient increase in Y is shelved but a sustained signal (while $\mathsf{w_B}$ is up) will overflow the shelves and allow translation of Xis, cf. Fig. 6. As a concrete mechanism we propose transcription of a repeated complement of Y, viz. $\langle \mathsf{w_A} \rangle \to (\mathsf{AraC}^*) \to [\mathsf{BAD}] \to (\mathsf{cI}^b) \dashv [\mathsf{cI}^b_{\_}] \to (\mathsf{Y}^*)^n \dashv \mathsf{Y} \to (\mathsf{Xis})$.

3 Simulations

3.1 General considerations

Recall from §2.3 that the dimerized (AmtR) represses [AmtR], which we can express as

$$2\,(\mathsf{AmtR}) + [\mathsf{AmtR}]_{\text{active}} \rightleftharpoons (\mathsf{AmtR})_2 : [\mathsf{AmtR}] = \text{repressed state}. \tag{5}$$

In steady state, we have the Hill equation

$$[\mathsf{AmtR}]_{\text{active}} = (1 + ((\mathsf{AmtR})/\mathrm{EC50})^n)^{-1}\,[\mathsf{AmtR}]_{\text{total}}. \tag{6}$$

In case of an activator we use, for example,

$$[\mathsf{Sal}]_{\text{active}} = (1 + (\text{EC50}/\langle \mathsf{Sal} \rangle)^n)^{-1} [\mathsf{Sal}]_{\text{total}}. \tag{7}$$

All species are in units of *molecules*. For simplicity, we use the above Hill equations (which, notably, have no baseline term) for all species with $n = 2$ and mostly EC50 $= 1$ molecules (cf. §4). We simulate production and degradation such that typically about 10 molecules of output from a fully active promoter correspond to the steady state, for example $\frac{\mathrm{d}}{\mathrm{d}t}(\mathsf{Output}) = k_+[\mathsf{Sal}]_{\text{active}} - k_-(\mathsf{Output})$ with $k_+ = 1\mathsf{s}^{-1}$ and $k_- = 0.1\mathsf{s}^{-1}$ models $[\mathsf{Sal}]_{\text{active}} \to (\mathsf{Output})$. Generally, we take 0.1 and 10 molecules to mean *off* and *on*, respectively. In the figures we refer to "a.u." instead of seconds, because these choices lead to timescales that are too fast to be realistic (perhaps by a factor of 10).

3.2 Player A

We implemented the response r_0 and r_1 of Player A in SymBiology as sketched out in §2.2. The steady-state response is shown in Fig. 4.

3.3 Bit 1

Carry flag c_2. We implemented c_2 in SymBiology as indicated in §2.2. Recall that c_2 is emitted immediately, bypassing the memory unit. Fig. 5 shows the steady-state response.

Difference d_1. We implemented d_1 in SymBiology as in §2.9 with the buffer/shelving mechanism (§2.10) and the recombinase memory unit (§2.7). Fig. 5 shows the write-then-emit response of this stack of circuits. Fig. 6 shows the time-course of key components over four phases (compute-read-compute-read) with a particular choice of inputs and illustrates the effect of shelving for isolating the memory unit from spurious output of the compute unit.

4 Discussion

The focus of this note is the design of a multi-cell genetic count-down computer which is *reusable*. Our solution relies on computing, remembering and emitting the new status in alternating phases. As part of the subtractor, we propose an RNA-based 3-XOR gate. The memory unit is based on a resettable recombinase. We also propose to insulate undesirable fluctuations in the output of the compute unit by means of a buffer (shelving).

Our simulations are highly stylized. For example, in reality, the EC50 of the signals vary over several orders of magnitude (Du et al., 2020, SM:Fig.8) and the Hill equation parameters depend on the context (Nielsen et al., 2016, SM:p.10); we rely on orthogonality of the signaling channels and ignore potential toxicity (Du et al., 2020, SM:p.8); we did not simulate diffusion of signaling molecules in/out of the cell nor systematically investigate robustness against mistiming of signaling.

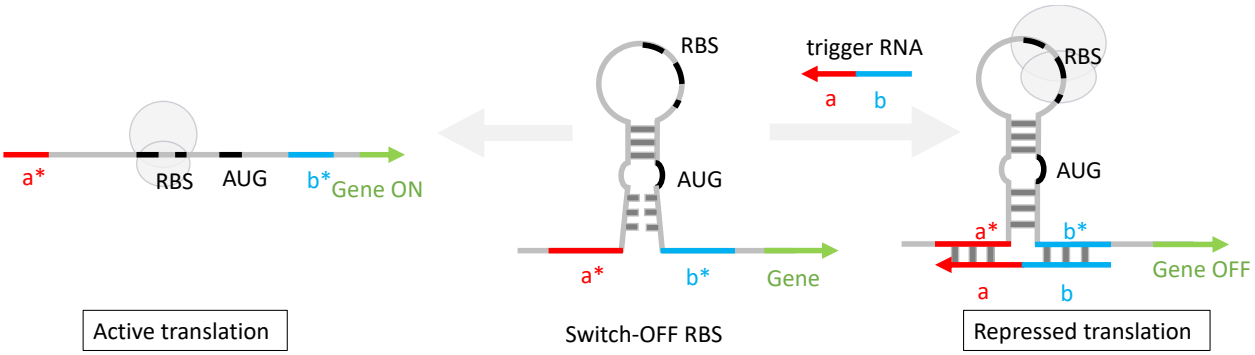

(a) The unstable hairpin is sealed by the trigger RNA ab, repressing translation. Adapted from (Kim et al., 2019, Fig. 1c).

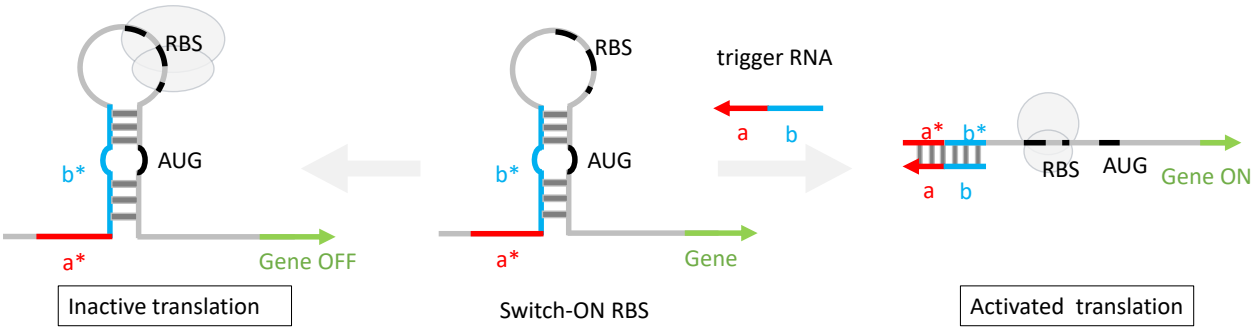

(b) The stem of the stable hairpin is opened by the trigger RNA ab, exposing the RBS for translation. Adapted from (Green et al., 2014, Fig. 1b).

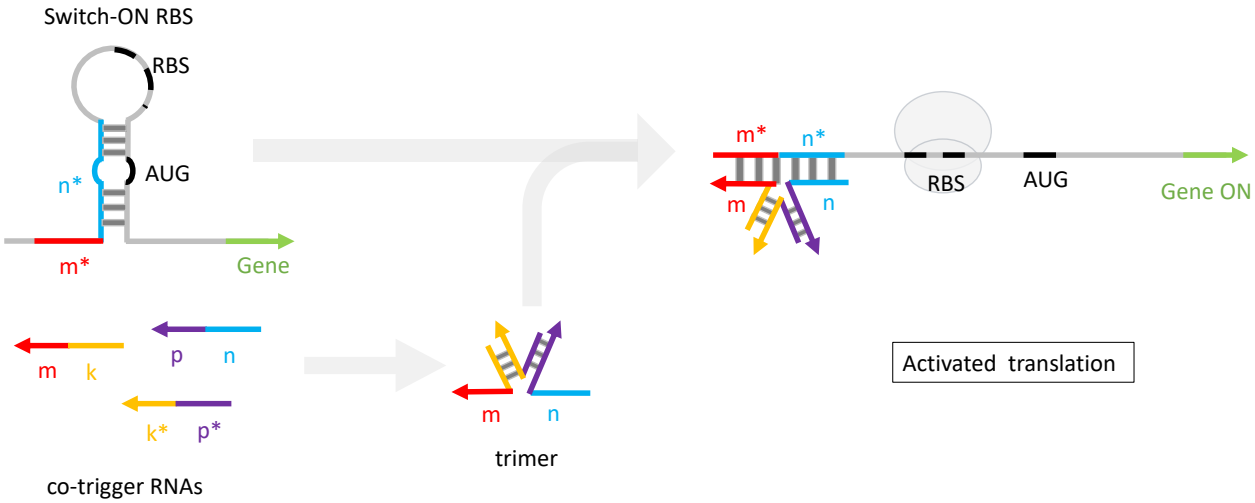

(c) The co-trigger RNAs form a trimer that switches ON the RBS. Adapted from (Green et al., 2017, Fig. 3a).

Figure 1: Switch-OFF (1a) and Switch-ON (1b) RBS; RNAs 3-AND gate (1c). Cf. §2.9/§2.8.

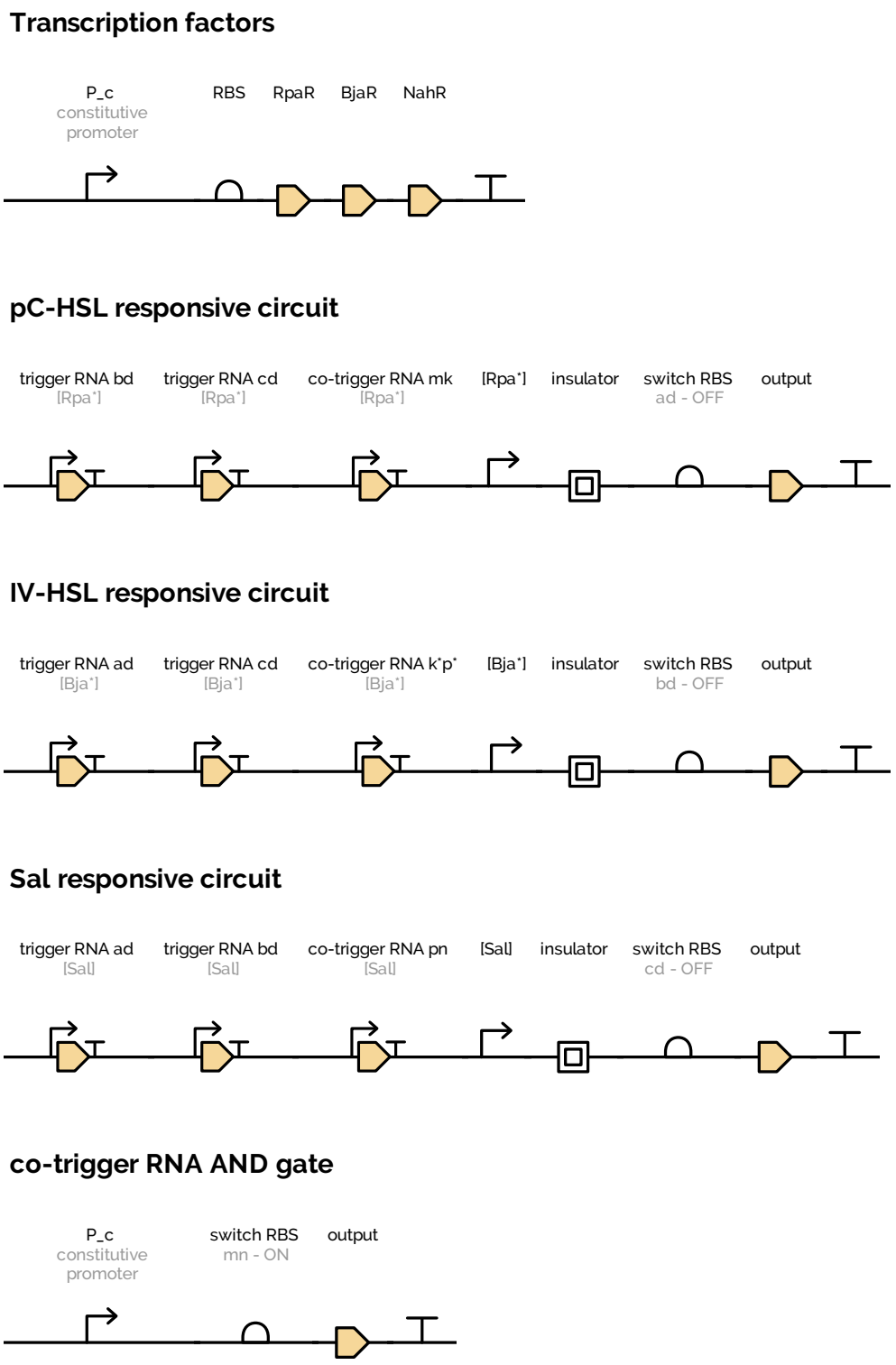

Figure 2: Genetic circuits for the 3-XOR DNF (4b) from §2.9. Cf. Fig. 3. Ribozyme insulators are placed just upstream of the switch RBS for non-constitutive promoters, see §2.4.

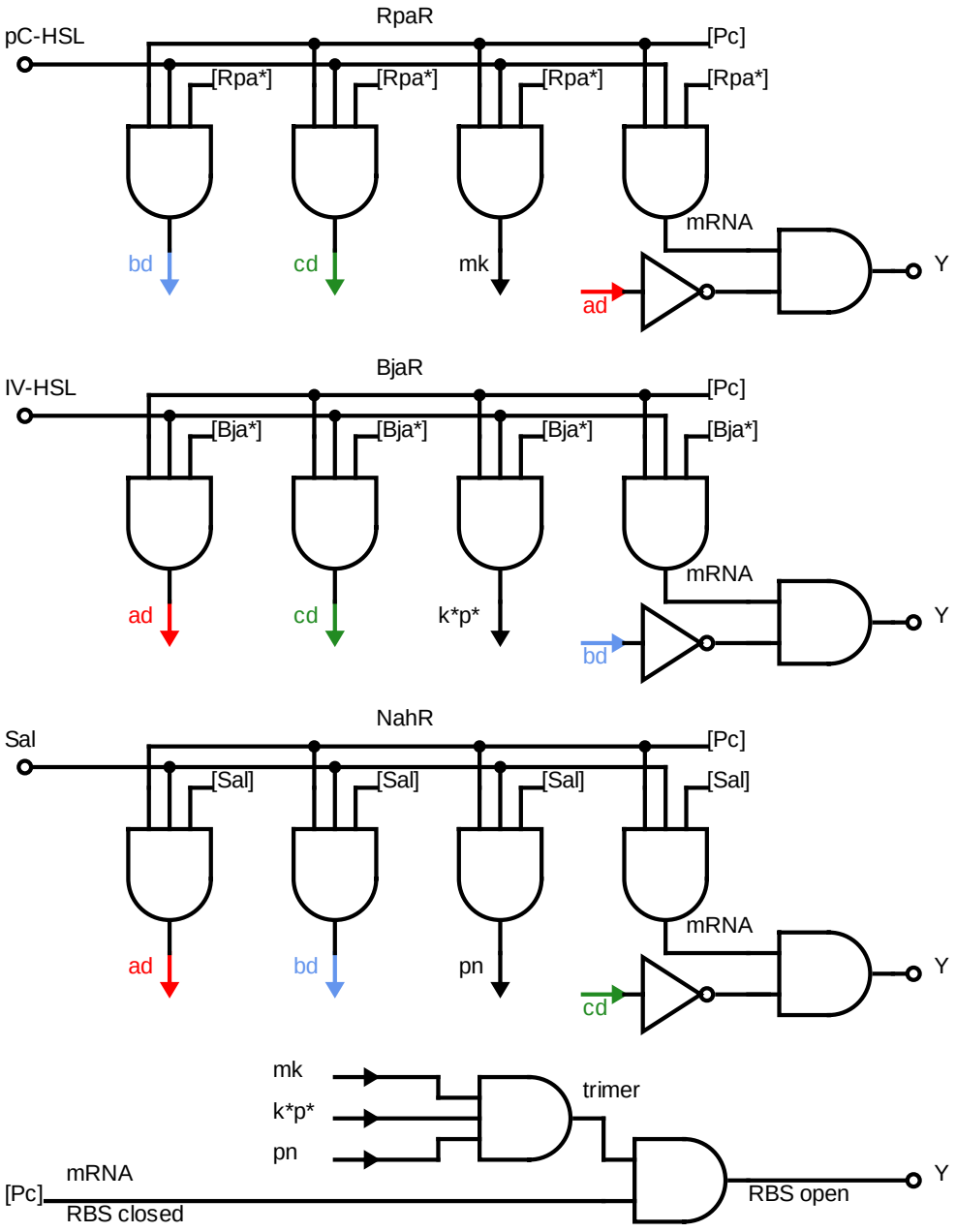

Figure 3: One-to-one logic gate representation of the genetic implementation of the 3-XOR DNF (4b) from §2.9. To avoid clutter the wiring is indicated by the arrows. Y indicates active output mRNA translation. Cf. Fig. 2.

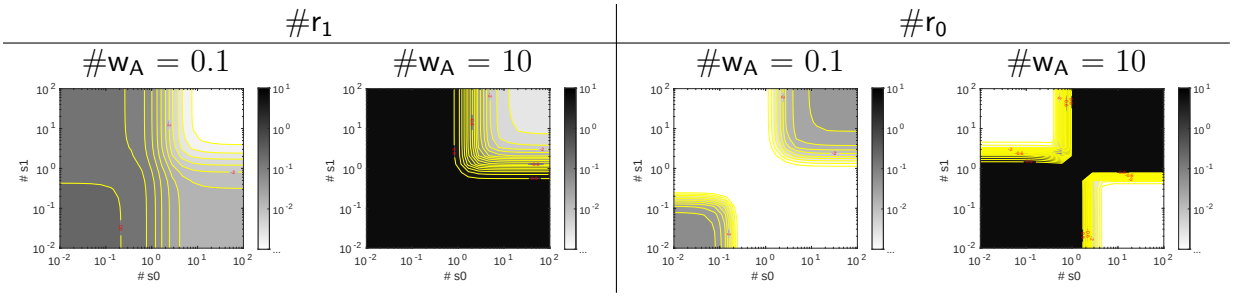

Figure 4: Response surfaces of Player A for varying $\#s_1(\uparrow)$ and $\#s_0(\rightarrow)$. See §3.2. The log-colorbar goes from 10^{-3}-or-less (white) to 10^{1} (black). Yellow contours at 10^{t}, $t = 0.8, 0.6, 0.4, \ldots$.

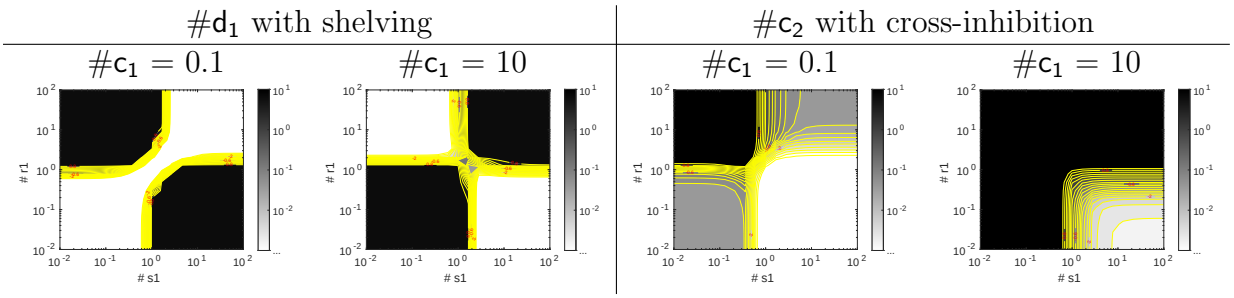

Figure 5: Response of Subtractor A for varying $\#r_1(\uparrow)$ and $\#s_1(\rightarrow)$. See §3.3. The output $\#d_1$ is measured after a compute-, inter- and readout-phase, cf. Fig. 6. The log-colorbar goes from 10^{-3}-or-less (white) to 10^{1} (black). Yellow contours at 10^{t}, $t = 0.8, 0.6, 0.4, \ldots$.

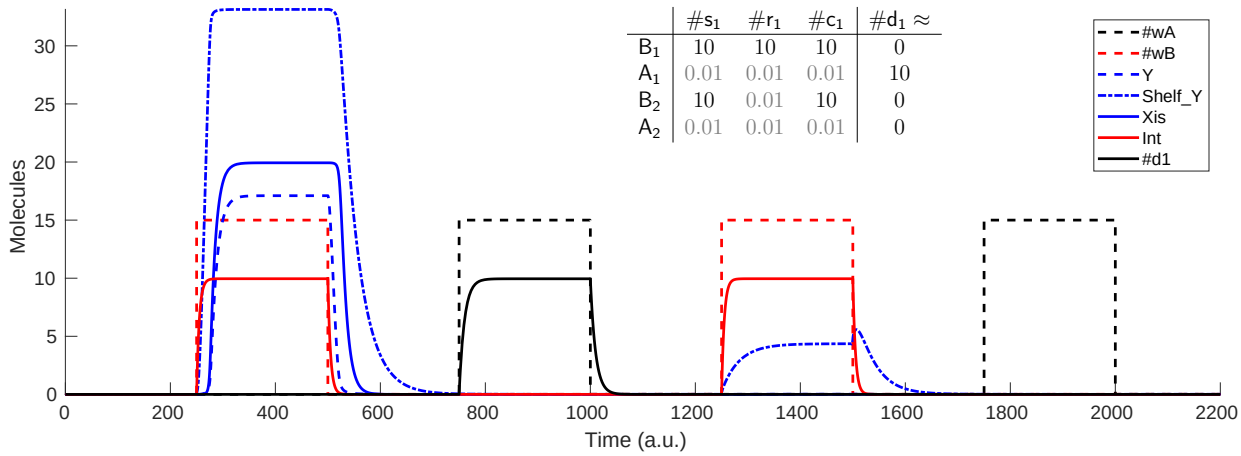

	$\#s_1$	$\#r_1$	$\#c_1$	$\#d_1 \approx$
B_1	10	10	10	0
A_1	0.01	0.01	0.01	10
B_2	10	0.01	10	0
A_2	0.01	0.01	0.01	0

Figure 6: Subtractor A, Bit 1, output $\#d_1$ across phases B_1-A_1-B_2-A_2 (with interphases). The table shows the inputs for each phase. We have $\#d_1 \approx 10$ in the recall phase A_1 and $\#d_1 \approx 0$ in A_2. Observe the slight delay in the rise of Y at the beginning of B_1 while it is being "shelved"; conversely, the leakage of Y is "shelved" during B_2 preventing unwanted expression of Xis. At the end of B_2, a small deliberate mistiming in signal decay leads to a bump in Y that is absorbed by the shelf. See also §3.3/p.11.

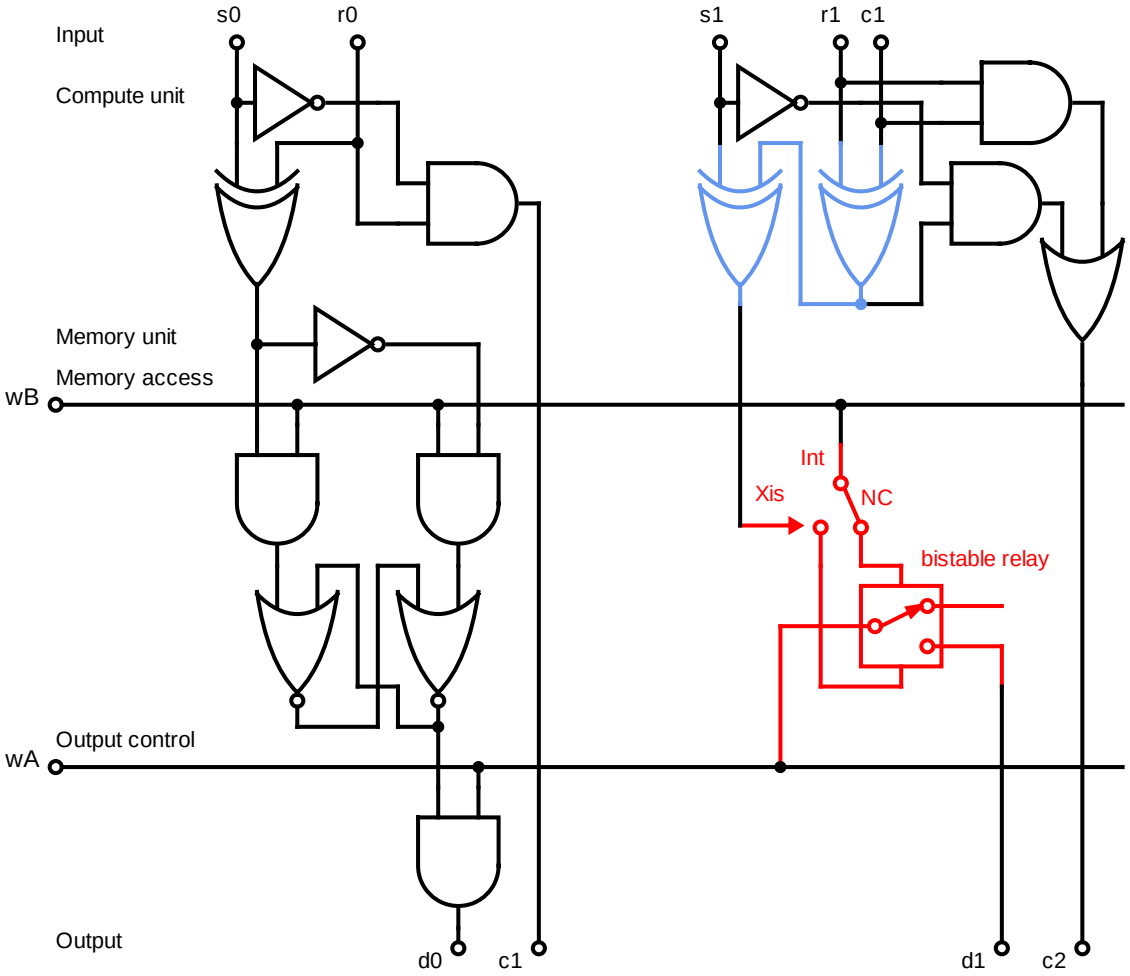

Figure 7: Conceptual/reference logic circuit of Bit 0 and Bit 1 of Subtractor A. The result of the compute unit is written to the memory unit when the signal w_B is present. The value of the memory unit is forwarded to the output when the signal w_A is present. The left part shows a possible implementation of the memory unit as a bistable switch with basic gates. The right part (in red) is closer to our actual genetic circuit using the reversible recombinase §2.7/p.8: the first relay (NC: normally closed) is switched temporarily by Xis; the bistable relay is switched stably by Int either up (from above) or down (from below), but remains unchanged without Int. The 3-XOR gate is shown (in blue) as two cascading XOR gates but we implement the DNF (4b), see Fig. 3.

References

Arkin, A., Ross, J., and McAdams, H. H. (1998). Stochastic kinetic analysis of developmental pathway bifurcation in phage λ-infected Escherichia coli cells. *Genetics*, 149(4):1633–1648.

Ausländer, D., Ausländer, S., Pierrat, X., Hellmann, L., Rachid, L., and Fussenegger, M. (2017). Programmable full-adder computations in communicating three-dimensional cell cultures. *Nature Methods*, 15(1):57–60.

Bangera, M. G. and Thomashow, L. S. (1999). Identification and characterization of a gene cluster for synthesis of the polyketide antibiotic 2,4-diacetylphloroglucinol from *Pseudomonas fluorescens* Q2-87. *Journal of Bacteriology*, 181(10):3155–3163.

Beckers, G., Strösser, J., Hildebrandt, U., Kalinowski, J., Farwick, M., Krämer, R., and Burkovski, A. (2005). Regulation of AmtR-controlled gene expression in *Corynebacterium glutamicum*: mechanism and characterization of the AmtR regulon. *Molecular Microbiology*, 58(2):580–595.

Bonnet, J., Subsoontorn, P., and Endy, D. (2012). Rewritable digital data storage in live cells via engineered control of recombination directionality. *Proceedings of the National Academy of Sciences*, 109(23):8884–8889.

Bottiglieri, M. and Keel, C. (2006). Characterization of PhlG, a hydrolase that specifically degrades the antifungal compound 2,4-diacetylphloroglucinol in the biocontrol agent *Pseudomonas fluorescens* CHA0. *Applied and Environmental Microbiology*, 72(1):418–427.

Brödel, A. K., Jaramillo, A., and Isalan, M. (2016). Engineering orthogonal dual transcription factors for multi-input synthetic promoters. *Nature Communications*, 7(1).

Carr, S. B., Beal, J., and Densmore, D. M. (2017). Reducing DNA context dependence in bacterial promoters. *PLOS ONE*, 12(4):e0176013.

Carrier, T. A. and Keasling, J. D. (1997). Engineering mRNA stability in *E. coli* by the addition of synthetic hairpins using a 5' cassette system. *Biotechnology and Bioengineering*, 55(3):577–580.

Chiu, T.-Y. and Jiang, J.-H. R. (2017). Logic synthesis of recombinase-based genetic circuits. *Scientific Reports*, 7(1).

Cuthbertson, L. and Nodwell, J. R. (2013). The TetR family of regulators. *Microbiology and Molecular Biology Reviews*, 77(3):440–475.

Du, P., Zhao, H., Zhang, H., Wang, R., Huang, J., Tian, Y., Luo, X., Luo, X., Wang, M., Xiang, Y., Qian, L., Chen, Y., Tao, Y., and Lou, C. (2020). De novo design of an intercellular signaling toolbox for multi-channel cell-cell communication and biological computation. *Nature Communications*, 11(1).

Egland, K. A. and Greenberg, E. P. (1999). Quorum sensing in *Vibrio fischeri*: elements of the luxI promoter. *Molecular Microbiology*, 31(4):1197–1204.

Fuqua, C., Winans, S. C., and Greenberg, E. P. (1996). Census and consensus in bacterial ecosystems: The LuxR-LuxI family of quorum-sensing transcriptional regulators. *Annual Review of Microbiology*, 50(1):727–751.

Grant, P. K., Dalchau, N., Brown, J. R., Federici, F., Rudge, T. J., Yordanov, B., Patange, O., Phillips, A., and Haseloff, J. (2016). Orthogonal intercellular signaling for programmed spatial behavior. *Molecular Systems Biology*, 12(1):849.

Green, A. A., Kim, J., Ma, D., Silver, P. A., Collins, J. J., and Yin, P. (2017). Complex cellular logic computation using ribocomputing devices. *Nature*, 548(7665):117–121.

Green, A. A., Silver, P. A., Collins, J. J., and Yin, P. (2014). Toehold switches: de-novo-designed regulators of gene expression. *Cell*, 159(4):925–939.

Hein, S., Hummel, N., Barthel, S., and Dohmen, T. (2014). *fdeR (Naringenin binding protein) and fde operon regulatory domain*. http://parts.igem.org/Part:BBa_K1497019.

Hirakawa, H., Oda, Y., Phattarasukol, S., Armour, C. D., Castle, J. C., Raymond, C. K., Lappala, C. R., Schaefer, A. L., Harwood, C. S., and Greenberg, E. P. (2011). Activity of the *Rhodopseudomonas palustris* p-coumaroyl-homoserine lactone-responsive transcription factor RpaR. *Journal of Bacteriology*, 193(10):2598–2607.

Huang, J. Z. and Schell, M. A. (1991). In vivo interactions of the NahR transcriptional activator with its target sequences. Inducer-mediated changes resulting in transcription activation. *Journal of Biological Chemistry*, 266(17):10830–10838.

Jakoby, M., Nolden, L., Meier-Wagner, J., Krämer, R., and Burkovski, A. (2000). AmtR, a global repressor in the nitrogen regulation system of *Corynebacterium glutamicum*. *Molecular Microbiology*, 37(4):964–977.

Kim, J., Zhou, Y., Carlson, P. D., Teichmann, M., Chaudhary, S., Simmel, F. C., Silver, P. A., Collins, J. J., Lucks, J. B., Yin, P., and Green, A. A. (2019). De novo-designed translation-repressing riboregulators for multi-input cellular logic. *Nature Chemical Biology*, 15(12):1173–1182.

Lindemann, A., Pessi, G., Schaefer, A. L., Mattmann, M. E., Christensen, Q. H., Kessler, A., Hennecke, H., Blackwell, H. E., Greenberg, E. P., and Harwood, C. S. (2011). Isovaleryl-homoserine lactone, an unusual branched-chain quorum-sensing signal from the soybean symbiont *Bradyrhizobium japonicum*. *Proceedings of the National Academy of Sciences*, 108(40):16765–16770.

Lou, C., Stanton, B., Chen, Y.-J., Munsky, B., and Voigt, C. A. (2012). Ribozyme-based insulator parts buffer synthetic circuits from genetic context. *Nature Biotechnology*, 30(11):1137–1142.

Muhl, D., Jeßberger, N., Hasselt, K., Jardin, C., Sticht, H., and Burkovski, A. (2009). DNA binding by *Corynebacterium glutamicum* TetR-type transcription regulator AmtR. *BMC Molecular Biology*, 10(1):73.

Nielsen, A. A. K., Der, B. S., Shin, J., Vaidyanathan, P., Paralanov, V., Strychalski, E. A., Ross, D., Densmore, D., and Voigt, C. A. (2016). Genetic circuit design automation. *Science*, 352(6281):aac7341.

O'Rourke, S., Wietzorrek, A., Fowler, K., Corre, C., Challis, G. L., and Chater, K. F. (2009). Extracellular signalling, translational control, two repressors and an activator all contribute to the regulation of methylenomycin production in *Streptomyces coelicolor*. *Molecular Microbiology*, 71(3):763–778.

Park, H. H., Lim, W. K., and Shin, H. J. (2005). In vitro binding of purified NahR regulatory protein with promoter psal. *Biochimica et Biophysica Acta (BBA) – General Subjects*, 1725(2):247–255.

Peking iGEM 2013 team (2013). *Biosensors: NahR*. http://2013.igem.org/Team:Peking/Project/BioSensors/NahR.

Ramos, J. L., Martínez-Bueno, M., Molina-Henares, A. J., Terán, W., Watanabe, K., Zhang, X., Gallegos, M. T., Brennan, R., and Tobes, R. (2005). The TetR family of transcriptional repressors. *Microbiology and Molecular Biology Reviews*, 69(2):326–356.

Salis, H. M. (2011). The ribosome binding site calculator. In *Methods in Enzymology*, pages 19–42. Elsevier.

Schaefer, A. L., Greenberg, E. P., Oliver, C. M., Oda, Y., Huang, J. J., Bittan-Banin, G., Peres, C. M., Schmidt, S., Juhaszova, K., Sufrin, J. R., and Harwood, C. S. (2008). A new class of homoserine lactone quorum-sensing signals. *Nature*, 454(7204):595–599.

Schell, M. A., Brown, P. H., and Raju, S. (1990). Use of saturation mutagenesis to localize probable functional domains in the NahR protein, a LysR-type transcription activator. *Journal of Biological Chemistry*, 265(7):3844–3850.

Schell, M. A. and Wender, P. E. (1986). Identification of the nahR gene product and nucleotide sequences required for its activation of the sal operon. *Journal of Bacteriology*, 166(1):9–14.

Schnider-Keel, U., Seematter, A., Maurhofer, M., Blumer, C., Duffy, B., Gigot-Bonnefoy, C., Reimmann, C., Notz, R., Défago, G., Haas, D., and Keel, C. (2000). Autoinduction of 2,4-diacetylphloroglucinol biosynthesis in the biocontrol agent *Pseudomonas fluorescens* CHA0 and repression by the bacterial metabolites salicylate and pyoluteorin. *Journal of Bacteriology*, 182(5):1215–1225.

Schuster, M., Urbanowski, M. L., and Greenberg, E. P. (2004). Promoter specificity in *Pseudomonas aeruginosa* quorum sensing revealed by DNA binding of purified LasR. *Proceedings of the National Academy of Sciences*, 101(45):15833–15839.

Schwab, C. (2019). *Characterization of transcription factor AmtR-DNA interaction*. PhD thesis, Friedrich-Alexander-Universität Erlangen-Nürnberg (FAU).

Sevvana, M., Hasselt, K., Grau, F. C., Burkovski, A., and Muller, Y. A. (2017). Similarities in the structure of the transcriptional repressor AmtR in two different space groups suggest a model for the interaction with GlnK. *Acta Crystallographica Section F Structural Biology Communications*, 73(3):146–151.

Siedler, S., Stahlhut, S. G., Malla, S., Maury, J., and Neves, A. R. (2014). Novel biosensors based on flavonoid-responsive transcriptional regulators introduced into *Escherichia coli*. *Metabolic Engineering*, 21:2–8.

Stevens, A. M., Dolan, K. M., and Greenberg, E. P. (1994). Synergistic binding of the *Vibrio fischeri* LuxR transcriptional activator domain and RNA polymerase to the lux promoter region. *Proceedings of the National Academy of Sciences*, 91(26):12619–12623.

Wang, B., Kitney, R. I., Joly, N., and Buck, M. (2011). Engineering modular and orthogonal genetic logic gates for robust digital-like synthetic biology. *Nature Communications*, 2(1).

Weinberg, B. H., Pham, N. T. H., Caraballo, L. D., Lozanoski, T., Engel, A., Bhatia, S., and Wong, W. W. (2017). Large-scale design of robust genetic circuits with multiple inputs and outputs for mammalian cells. *Nature Biotechnology*, 35(5):453–462.

Wong, A., Wang, H., Poh, C. L., and Kitney, R. I. (2015). Layering genetic circuits to build a single cell, bacterial half adder. *BMC Biology*, 13(1).

Zhou, S., Bhukya, H., Malet, N., Harrison, P. J., Rea, D., Belousoff, M. J., Venugopal, H., Sydor, P. K., Styles, K. M., Song, L., Cryle, M. J., Alkhalaf, L. M., Fülöp, V., Challis, G. L., and Corre, C. (2020). Structural basis for control of antibiotic production by bacterial hormones. *bioRxiv*. 2020.05.02.073981v1.